Applied Energy 159 (2015) 145–160

Contents lists available at ScienceDirect

Applied Energy

journal homepage: www.elsevier.com/locate/apenergy

Series–Parallel PV array re-configuration: Maximization of the extraction of energy and much more

M. Balato, L. Costanzo *, M. Vitelli

Department of Industrial and Information Engineering, Second University of Naples, Aversa 81031, Italy

HIGHLIGHTS

- A new fast re-configuration algorithm for Series–Parallel architecture is proposed.
- Main advantage: fast identification of a nearly optimal configuration.
- The dynamical re-configuration allows the maximization of the extracted energy.
- Maximum efficiency and premature aging are contrasting requirements.

ARTICLE INFO

Article history:
Received 23 December 2014
Received in revised form 7 May 2015
Accepted 17 August 2015
Available online 10 September 2015

Keywords:
Mismatching
Photovoltaic array re-configuration
Series–Parallel architecture

ABSTRACT

In this paper a simple and fast re-configuration algorithm which is suitable for a PV array with Series–Parallel architecture is presented and discussed. The main advantage of such an algorithm is represented by its capability to find a nearly optimal configuration by testing only a very small subset of all the possible configurations. In particular it is shown that, in an actual PV array composed by 24 PV modules which operate under mismatching conditions (which are quite common in urban environments due to chimneys, streets lighting poles, antennas, neighboring buildings, etc.), the proposed algorithm is able to lead to energetic performances which are more or less comparable with those ones which can be obtained by adopting a Monte Carlo based algorithm employing a much higher number of trials. Moreover, by means of a specific example, it is shown that maximization of extracted energy and absence of dangerous operating conditions, possibly leading to the premature aging of the PV field and/or to hot spot phenomena, are contrasting requirements. It is nonetheless possible to find proper configurations able to lead to a suitable compromise between such two contrasting requirements. Further work is needed and is in progress in order to design suitable re-configuration algorithms able to identify such compromise configurations.

1. Introduction

In PV applications the main cause of waste of available energy is represented by mismatching operating conditions. Mismatch can be originated by shadows produced by clouds or by neighboring objects or buildings [1], dirtiness [2], manufacturing tolerances, aging, different orientation of parts of the PV field [3–6], thermal gradients [7], etc. In mismatching operating conditions, the Power versus Voltage (*P–V*) characteristic of a PV field may exhibit more than one peak, therefore Maximum Power Point Tracking (MPPT) algorithms [8–13] (such as the "Perturb & Observe" algorithm) may fail since the operating point of the system may remain trapped in the neighborhood of a relative Maximum Power Point (MPP) instead that close to the absolute MPP [14–18]. Moreover, even when the MPPT algorithm is able to track the absolute MPP of the mismatched PV field, the extracted power is lower than the sum of the available maximum powers that the mismatched modules are able to provide [19]. The so called Distributed Maximum Power Point Tracking (DMPPT) architectures allow to overcome the drawbacks associated to mismatching phenomena. DMPPT architectures are based on the adoption of module dedicated dc/dc converters [20–28], or on the adoption of module dedicated dc/ac converters [29–37] which perform the MPPT of each PV module, instead that the MPPT of the whole PV array. The main drawbacks of DMPPT architectures are the high cost and, in the case of module dedicated dc/dc converters, the reduced plant efficiency during the day hours in which the PV array operates under a uniform irradiation level. In such conditions the overall efficiency of the system is lowered, with respect to the case

* Corresponding author.
E-mail address: luigi.costanzo@unina2.it (L. Costanzo).

http://dx.doi.org/10.1016/j.apenergy.2015.08.073
0306-2619/

of central MPPT PV architectures, due to the power stage efficiency of the module dedicated dc/dc converters which have to process anyhow the whole PV power. Moreover, both the dc/dc and the dc/ac module dedicated converters introduce further components (e.g. large electrolytic capacitances) that may reduce the system reliability and hence its lifetime [38,39]. An alternative solution able to mitigate the drawbacks associated to mismatching operating conditions is represented by the dynamical re-configuration of PV arrays by means of proper active switches. The re-configuration approach is characterized by the significant advantage, with respect to the DMPPT architectures, of reducing to zero the power which is wasted when the PV field works in uniform operating conditions. The lack of DMPPT dc/dc converters, that process the PV power also when this is not necessary at all, undoubtedly increases the efficiency of the whole PV system. In presence of mismatching instead, by means of a proper control of the switches matrix, the best configuration of the PV modules can be obtained in order to maximize the energy extraction. Thus, the re-configuration solution certainly outperforms the DMPPT solution in the frequent cases of PV systems which are characterized by shadowing taking place during only some parts of the day. As an example in case of shadows (caused by poles, small walls or buildings) which occur only at sunrise and/or sunset, while during the central part of the day the PV field works without mismatching. It is worth noting that, already many years ago, extensive numerical studies related to the applicative domain of small-power irrigation plants have emphasized the validity of the matching technique based on the direct connection of the load to a variable geometry PV generator [40]. In mismatching conditions, the efficiency obtainable by means of array dynamical re-configuration turns out to be more or less comparable with the efficiency which is obtained by means of sophisticated DMPPT architectures providing source-load matching by means of electronic interfaces. Of course, the improvement in coupling efficiency expected over static architectures based on an optimally designed but fixed architecture PV generator which is directly connected to the load is, on the other hand, remarkable [41]. It therefore seems reasonable to conclude that the superior energetic performance achievable in the long term amply repays the additional hardware necessary to assemble and control a re-configurable PV generator, provided that a reasonable number of switches is used. This is a crucial point. In the literature, a number of theoretical and numerical analyses on reconfiguration techniques requiring unpractical and unrealistically large number of switches have been presented and discussed. But, in order to be really used in practical applications, reconfiguration techniques must be based on a limited number of switches. As discussed in Section 2, the re-configuration technique which is analyzed in this paper is based on the Series–Parallel (SP) connection of the PV modules (which can be arranged in two parallel connected strings) and requires a much lower number of switches in comparison to reconfiguration techniques adopting Totally-Cross-Tied (TCT) or other complex architectures [42–49]. It is worth noting that, apart from the maximization of the extracted energy, the additional hardware required by re-configurable PV arrays also offers other opportunities. In fact, it should be considered also the support that a microprocessor-based controller provides for automatic detection of failures by exploiting the individual measurement of each PV module's current vs. voltage (I–V) curve or the knowledge of other PV module parameters (such as the short circuit current, the open circuit voltage, the temperature, etc.) which are needed for the working of the various re-configuration strategies presented in the literature [50–53]. This powerful built-in diagnostic capability further enhances overall system reliability and efficiency. Moreover, a proper control of the matrix of switches allows to avoid dangerous voltages during installation, emergency (e.g. in case of fire, thus protecting firemen) or maintenance (thus protecting technicians). Summarizing, the dynamic array re-configuration solution is cheaper than the one involving power optimizers, provided that a reasonable number of switches is used, and, besides the possibility of plant monitoring, offers additional advantages in terms of safety in case of fire or maintenance. A further aspect which, to the best of the authors' knowledge, has not been investigated in the literature is represented by the possibility to re-configure the PV modules in order to obtain a kind of multi-objective optimization. In particular, it is possible to get a trade-off between the extracted energy and the increase of the expected life of the PV modules. In fact, the PV modules connections can be re-configured in such a way that it is possible, not only to extract higher energy with respect to the case of static architectures, but also to limit or, in some cases, to entirely avoid the occurrence of phenomena (such as the so-called hot spot) leading to the premature aging or even to the failure of one or more PV modules of the array. In practice, it is possible to exclude one or more configurations which, although characterized by very high extracted powers, also lead to enhanced electrical and thermal stresses of the PV modules. Such a specific aspect will be the subject of Section 5 of this paper. The general conclusions which can be drawn from the research activity are reported in Section 6.

2. Why SP re-configuration

Although many interconnection topologies have been developed in the literature, so far the most exploited solutions rely on SP and TCT module interconnections [49]. In actual PV power plants, the SP is by far the most common connection. It is obtained by connecting solar modules in series in order to form strings which are able to provide the voltage required by the inverter; such strings are then connected in parallel to increase the total current. In TCT configurations, PV modules are first parallel tied so that their voltages are equal and their currents are summed up; a number of these rows of modules are then connected in series. Though under uniform conditions SP and TCT modules connections provide nearly the same power value, in mismatching conditions the TCT topology usually exhibits better energetic performances with respect to the SP topology [41]. On the other hand, as stated in Section 1, an important aspect to consider, when dealing with re-configurable PV architectures, is represented by the required number of switches and sensors and by the complexity of the re-configuration algorithms. In particular, nearly all the proposed re-configuration methods based on the TCT topology need an unrealistic number of sensors and switches [49]. As an example, the switching matrix of the system discussed in [41] is composed by N_{PV}^2 double-pole switches plus N_{PV} single-pole switches, where N_{PV} is the number of the PV modules. Such a switching matrix allows all the configurations between the two extreme cases of all parallel-connected modules configuration (all modules stay in a single row) and all series-connected modules configuration (one module per row). In a system composed by $N_{PV} = 24$ PV modules, 600 switches would be necessary. As an additional example, in [48] the switch structure requires an even higher number of switches equal to $2 \cdot N_{PV}^2$ (1152 switches). Moreover, nearly all the proposed re-configuration methods based on the TCT topology use quite complex control algorithms to determine when to turn the switches on or off. Such control algorithms often require an unpractical number of calculations [49]. As an example, in [41] $(N_{PV} \cdot N_{PV})!/(N_{PV}!)^{NPV}$ different configurations are possible and need to be considered (with $N_{PV} = 24$ the previous expression leads to an overflow in MATLAB). It is clear that, in practice, commercial TCT arrays cannot be easily, effectively and efficiently controlled. It is a matter of fact that, to the best of the authors' knowledge, the only commercial device (ENDANA by BITRON) allowing the reconfiguration of a PV array is based on the SP topology [54]. The basic version of ENDANA is able to re-configure 24 PV modules in 2 strings. ENDANA measures the full Power vs. Voltage (*P–V*) curve of each PV module and reconfigures module connections into two substrings, while excluding, if necessary, some strongly shaded PV modules. On the basis of the above considerations, we have chosen to focus the attention on the SP topology also because, with such a topology, it is possible, at least in principle, to carry out the retrofit on most existing PV fields. An important additional aspect to emphasize is that, in most cases, the reconfiguration of the TCT topology is analyzed by considering PV units which are simply represented by strings of PV cells and by neglecting the possible presence of multiple maxima in the *P–V* characteristics of one or more of such strings. In commercial PV modules instead, each string of cells is protected by its own bypass diode and a partial shadowing affecting the module often leads to the appearance of multiple MPPs. In almost all papers dealing with re-configuration algorithms to be applied to TCT architectures, the problem of the multi-modality of the *P–V* curves is not afforded at all and the algorithms are usually based on the knowledge of short-circuit currents only. In the following, we will discuss a re-configuration algorithm which is suitable for the SP connection of commercial PV modules. It is based on the knowledge of the full *I–V* characteristic of each PV module in order to correctly face the eventual occurrence of multiple MPPs in the *P–V* characteristics of one or more PV modules. We explicitly remark here that the aim of this paper is not to carry out a comparison between performances provided by re-configuration strategies applied to TCT and to SP topologies. Instead, we will discuss a very simple Heuristic algorithm that, whichever the mismatching conditions, can quickly identify proper SP configurations able to provide greater power with respect to a fixed SP architecture. The main features of the proposed algorithm are represented just by the simplicity of implementation and by the speed of execution.

3. Proposed re-configuration algorithm

In the following, for the sake of simplicity but without any loss of generality, a SP PV field made of N_{PV} ($N_{PV} = 24$) modules distributed among two strings will be considered. This is the same configuration adopted by ENDANA [54]. Most residential PV arrays in Italy are characterized by such an architecture. Each PV module may be put into one of the two strings or may be disconnected. Therefore the *j*-th PV module will be assigned to an index q_j: $q_j = 0$ means that the *j*-th PV module is disconnected from the PV field; $q_j = 1$ means that it is connected to the first string; $q_j = 2$ means that it is connected to the second string. In particular, a configuration vector *C* with N_{PV} components collects the above information; the *j*-th component $C(j)$ of *C* is equal to q_j. Of course, the total number of possible configuration vectors *C* is equal to 3^{NPV}. However, since one theoretical configuration vector is made of all zeros (all the panels are disconnected) and the configurations in which the panels are swapped between the two strings are equivalent, the number N_{TOT} of theoretical different configuration vectors of interest is indeed equal to $N_{TOT} = (3^{NPV} - 1)/2$. With $N_{PV} = 24$ we get $N_{TOT} = 1.412 \cdot 10^{11}$, which is a huge number of configurations. In practice however, inverter constraints must be taken into account. In fact, each inverter is characterized by its own MPPT voltage range [V_{inv_min}, V_{inv_max}], that is a voltage range, provided by the manufacturer, where the inverter is able to perform the MPPT operation. Therefore, as an example, all the PV modules configurations which are characterized by an open circuit voltage V_{oc_array} which is lower than V_{inv_min} are useless. Moreover, for obvious safety reasons, all the PV modules configurations which are characterized by an open circuit voltage V_{oc_array} which is higher than the inverter input voltage rating V_{inv_rating} must also be discarded. Summarizing, the number of configurations which comply with the inverter constraints is indeed lower than N_{TOT} but it is not possible to a priori exclude all the useless or dangerous configurations since it is nearly impossible to identify them in advance. However, even if it was possible to identify and exclude them, an exhaustive search of the optimal configuration among the remaining inverter complying configurations would be unfeasible in any case. It should be taken into account that the identification of the optimal configuration must be carried out in real time during the day, since the shadowing pattern on the PV field may continuously change during the day. This requires suitable and fast techniques for monitoring the working condition of each PV module and for optimizing the connections among the PV modules without being forced to evaluate all the possibilities. In fact these are too many to be evaluated, in a reasonable amount of time, by means of a digital processor like a DSP or an FPGA. It should be taken into account that, of course, the larger the time needed for the optimization, the lower the frequency of reconfigurations and consequently the higher the probability to miss the possibility of adapting in time the module connections to the moving shadows. In the following, the best configuration vector provided by the re-configuration algorithm which is proposed in this paper will be identified with the symbol C_{OPT}. As discussed in Section 4, C_{OPT} is indeed a suboptimal solution rather than the optimal one. However C_{OPT} can be identified in a quite fast manner, by means of the analysis of a very limited number of configurations and the proposed algorithm allows to obtain a very good tradeoff between speed of operation and maximum extracted power. On the basis of the previous considerations, the proposed deterministic reconfiguration algorithm is made of four steps:

Step 1: The tracing of the *I–V* curve of the *j*-th module ($j = 1, 2, \ldots, N_{PV}$) is carried out by means of suitable measurement devices. In the following, it will be assumed that the *I–V* curve of the *j*-th module is obtained by collecting N_j samples which are uniformly spaced in current and that have coordinates ($V_{j,k}$; $I_{j,k}$) $k = 1, 2, \ldots, N_j$; $j = 1, 2, \ldots, N_{PV}$. Where $V_{j,k}$ ($I_{j,k}$) represents the *k*-th voltage (current) sample of the *I–V* curve of the *j*-th PV module. In particular the symbol ΔI ($\Delta I > 0$) will be used to identify the absolute value of the difference between the current values of two consecutive samples:

$$\Delta I = I_{j,k} - I_{j,k+1} \tag{1}$$

Of course, once the *I–V* curve is known, it is very easy to get the power vs. current (*P–I*) characteristic which is composed by N_j samples which are uniformly spaced in current and that have coordinates ($I_{j,k}$; $P_{j,k} = I_{j,k} \cdot V_{j,k}$) $k = 1, 2, \ldots, N_j$; $j = 1, 2, \ldots, N_{PV}$.

Step 2: The PV module which is characterized by the largest area *A* enclosed between the *P–I* curve and the *I*-axis is identified. Let's suppose that the *b*-th module exhibits the largest area A_b. Expression (2) provides an approximate value of such an area:

$$A_b = \sum_{k=1}^{N_b} P_{b,k} \cdot \Delta I \tag{2}$$

where N_b is the total number of samples of the *b*-th *P–I* curve. The *b*-th module is therefore characterized, with respect to the other PV modules, by a quite large average power in a quite large current range. Intuitively, these features are highly desirable for a PV module to be inserted in a string, if the aim is represented by the maximization of the extracted power. Heuristically speaking, the *b*-th module must therefore be preferred to any other module which is instead characterized by a lower average power and/or a lower current operating range and hence a lower area *A*.

Step 3: Subsequently, the N_{PV} modules are ordered in ascending order on the basis of the indicator χ_j defined, with the usual meaning of symbols, as:

$$\chi_j = \sum_{k=1}^{\max(N_j,N_b)} |P_{b,k} - P_{j,k}| \tag{3}$$

Since in general, in the above expression, it is $N_j \neq N_b$, the one of the two curves for which less samples are available will be augmented with a number of samples equal to zero. That is, if $N_j > N_b$ then $P_{b,k} = 0$ for $k = N_b + 1, \ldots, N_j$; if instead $N_b > N_j$ then $P_{j,k} = 0$ for $k = N_j + 1, \ldots, N_b$. In practice, the lower χ_j the lower the cumulative distance between the *P–I* curves of the *b*-th module and of the *j*-th module. If such two modules must be connected in series, it is highly desirable that χ_j is as low as possible since this implies that the *P–I* curves of the *b*-th module and of the *j*-th module match well. The ideal situation is when $\chi_j = 0$ since, in such a case, the *b*-th and the *j*-th *P–I* characteristics are exactly coincident and no mismatching exists between them. It is worth noting that the algorithm processes the *P–I* characteristics (and not the *P–V* characteristics) because the PV modules must be arranged in series to form a string. Should they be connected in parallel instead, then the *P–V* characteristics should be considered.

Step 4: It is worth noting that, once the *I–V* experimental characteristics of two or more PV modules are known, then the evaluation of the equivalent *I–V* characteristic of their series connection is very easy. As written above, the *I–V* experimental characteristic of the *j*-th module is obtained by collecting N_j samples with coordinates $(V_{j,k}; I_{j,k})$ $k = 1, 2, \ldots, N_j$; $j = 1, 2, \ldots, N_{PV}$. Obviously the experimental *I–V* characteristic is indeed a discrete rather than a continuous curve. However it can be easily converted into a continuous curve $V = f_k(I)$ by means of a proper interpolation of the starting samples. In particular, a linear interpolation has been used since it is enough accurate for the considered application. Once the continuous interpolated expression $V = f_k(I)$ is available, it is very easy to obtain the equivalent *I–V* characteristics of the two strings. They are: $V = \text{å}_{r1} f_{r1}(I)$ for String 1 and $V = \text{å}_{r2} f_{r2}(I)$ for String 2, where $r1$ ($r2$) represents the indices of all the PV modules belonging to String 1 (2). That is, due to the series connection of the PV modules of a given string, in order to get the *I–V* string characteristic it is enough, in correspondence of the same current value, to sum the corresponding values of the PV modules voltages. Moreover, once the *I–V* characteristics of the two different strings of modules are known, then the evaluation of the equivalent *I–V* characteristic of their parallel connection is very easy. It is preliminarily convenient to convert the *I–V* string characteristics in the form $I = g_1(V)$ for String 1 and $I = g_2(V)$ for String 2. This can be easily done by carrying out a scan of the two *I–V* string characteristics in order to collect samples which are uniformly spaced in current and, afterwards, by means of a proper linear interpolation of such samples. The *I–V* characteristic of the whole array is given by $I = g_1(V) + g_2(V)$ since, due to the parallel connection of the two strings, it is necessary, in correspondence of the same voltage value, to sum the corresponding values of the currents. It is worth noting that the above process can be carried out whichever is the final, resulting number of local maxima of the *P–V* characteristic of the whole array. In other words, no a priori knowledge of the total number of the local maxima of the *P–V* characteristic is required at all.

Summarizing, once the N_{PV} modules are distributed among the two strings, if the N_{PV} individual *I–V* characteristics of the modules are known, it is very easy to get the equivalent *P–V* characteristic of the whole PV array. Step 4 is used to analyze a subset of all the possible N_{TOT} configurations in order to identify C_{OPT}. In particular, such a subset is composed by N_{SUBSET} ($N_{SUBSET} < N_{TOT}$) different configurations:

$$N_{SUBSET} = N_{MAX} - (N_{PV} - N_{MIN}) + \sum_{r=1}^{N_{PV}-2N_{MIN}+1} r \tag{4}$$

where N_{MIN} (N_{MAX}) is the minimum (the maximum) number of PV modules which, when connected in series, are characterized by an open circuit voltage higher than V_{inv_min} (lower than V_{inv_rating}). In particular it is: $N_{MIN} = V_{inv\_min}/V_{oc\_max}$ and $N_{MAX} = V_{inv\_max}/V_{oc\_min}$ where V_{oc_max} (V_{oc_min}) is the maximum (minimum) value of the modules' open circuit voltages. It is worth remembering that the PV modules have been ordered in ascending order on the basis of the indicator χ_j which has been previously defined. In practice, as shown in Table 1 where the analyzed configurations are schematically reported, the first N_{MIN} modules are initially put in the String 1. Such modules are the N_{MIN} modules which, among the N_{PV} modules, exhibit less mismatching with respect to the *b*-th reference module and, at the same time, they are able to provide a string voltage falling in the interval $[V_{inv\_min}, V_{inv\_max}]$. The remaining modules are put in the String 2 if $(N_{PV} - N_{MIN}) \leqslant N_{MAX}$; otherwise, if $(N_{PV} - N_{MIN}) > N_{MAX}$, only those modules with indices belonging to the range $[N_{MIN} + 1, N_{MIN} + N_{MAX}]$ are put in the String 2 (in order to comply with the inverter input voltage rating) and the remaining ones are disconnected from both strings. This is the first *analyzed* configuration. With the terms "*analyzed*" configuration we mean a configuration for which the maximum value P_{MPP} of the power provided in the voltage range $[V_{inv\_min}, V_{inv\_max}]$ and the corresponding voltage value V_{MPP} are recorded. This task can be easily carried out, as explained above, once the *I–V* characteristics of the PV modules assigned to the two strings are known. Afterwards, the second configuration is *analyzed*. Such a configuration is obtained from the first one by freezing String 1 and, at the same time, by cutting from the String 2 the PV module with the highest value of the index. Such a module will be disconnected from both strings. The above process is repeated until the number of modules belonging to String 2 becomes equal to N_{MIN}. At this point the number of modules assigned to the String 1 is augmented to $N_{MIN} + 1$. The remaining modules are put in the String 2 if $[N_{PV} - (N_{MIN} + 1)] \leqslant N_{MAX}$; otherwise, if $[N_{PV} - (N_{MIN} + 1)] > N_{MAX}$, only those modules with indices belonging to the range $[N_{MIN} + 2, N_{MIN} + 2 + N_{MAX}]$ are put in the String 2. Such a configuration is analyzed together with all those

Table 1
Configurations analyzed by the proposed re-configuration algorithm.

PV modules assigned to String 1	PV modules assigned to String 2	
$1, 2, \ldots, N_{MIN}$	If $(N_{PV} - N_{MIN} \leqslant N_{MAX})$	$N_{MIN} + 1, \ldots, N_{PV} - i \quad i = 0, 1, \ldots, N_{PV} - 2N_{MIN}$
	If $(N_{PV} - N_{MIN} > N_{MAX})$	$N_{MIN} + 1, \ldots, (N_{MIN} + N_{MAX}) - \quad i \quad i = 0, 1, \ldots, N_{MAX} - N_{MIN}$
$1, 2, \ldots, N_{MIN} + 1$	If $[N_{PV} - (N_{MIN} + 1) \leqslant N_{MAX}]$	$N_{MIN} + 2, \ldots, N_{PV} - i$ with $i = 0, 1, \ldots, N_{PV} - 2N_{MIN} - 1$
	If $[N_{PV} - (N_{MIN} + 1) > N_{MAX}]$	$N_{MIN} + 2, \ldots, (N_{MIN} + 1 + N_{MAX}) - i$ with $i = 0, 1, \ldots, N_{MAX} - N_{MIN}$
....	....	
$1,2, \ldots, N_{MAX}$	If $(N_{PV} - N_{MAX} \leqslant N_{MAX})$	$N_{MAX} + 1, \ldots, N_{PV} - i \quad i = 0, 1, \ldots, N_{PV} - N_{MAX} - N_{MIN}$
	If $(N_{PV} - N_{MAX} > N_{MAX})$	$N_{MAX} + 1, \ldots, 2N_{MAX} - i \qquad i = 0, 1, \ldots, N_{MAX} - N_{MIN}$

Table 2
Example of configurations analyzed by the proposed re-configuration algorithm.

PV modules assigned to String 1	PV modules assigned to String 2	Number of analyzed configurations
1, 2, . . . , 5	6, 7, 8, . . . , 24 6, 7, 8, . . . , 23 6, 7, 8, . . . , 22 . . . . 6, 7, 8, . . . , 10	15
1, 2, . . . , 6	7, 8, 9, . . . , 24 7, 8, 9, . . . , 23 7, 8, 9, . . . , 22 . . . . 7, 8, 9, . . . , 11	14
1, 2, . . . , 7	8, 9, 10, . . . , 24 8, 9, 10, . . . , 23 8, 9, 10, . . . , 22 . . . . 8, 9, 10, . . . , 12	13
. . . .	. . . .	
1,2, . . . , 20	No PV modules, ($N_{PV} - N_{MAX} = 4 < N_{MIN}$)	1

configurations obtained by progressively cutting one module at a time (the last one) from String 2. The above process is repeated until the number of modules belonging to String 2 becomes equal to N_{MIN}. The algorithm goes on, by using the rules described above, until all the configurations obtained by freezing the first N_{MAX} PV modules in the String 1 have been analyzed. For example, if we consider $N_{MIN} = 5$ and $N_{MAX} = 20$ ($N_{PV} - N_{MIN} < N_{MAX}$), the configurations analyzed by the proposed re-configuration algorithm are reported in Table 2. We explicitly remark here that the simple deterministic algorithm described above is able to provide not only the configuration vector C_{OPT}, but also the corresponding optimal operating value V_{MPP} of the voltage. This information is extremely useful for the controller of the inverter which is fed by the PV array. In fact, in this way there is no chance for the inverter MPPT algorithm to be deceived by the eventual presence of multiple maxima in the total *P–V* characteristic of the array.

The best way to illustrate the performances of the proposed algorithm would be to compare such performances with those ones exhibited by a benchmark re-configuration algorithm. The problem is that, to the best of the authors' knowledge, even if a huge number of re-configuration algorithms have been proposed in the literature, most of them work with TCT or other complicated architectures. In any case, up to now, a benchmark algorithm does not exist, whichever the adopted architecture (SP or TCT). In fact, in almost all papers dealing with re-configuration algorithms no theoretical proof has ever been provided which demonstrates the capability of a given algorithm to find the real optimal solution without errors. Rather, nearly all the algorithms are able to find suboptimal solutions. The energetic performances of re-configuration strategies are usually compared with those ones obtained by adopting static configurations. On the basis of the above considerations, the energetic performances of the optimal configuration which is found by using the proposed algorithm will be compared not only with those ones obtained by adopting a static PV array configuration but also with those ones obtained by adopting a re-configuration strategy based on a simple Monte Carlo (MC) search. Of course, the number N_{trials} of MC trials represents the number of *analyzed* configurations by the MC search. It is well known that the higher N_{trials} the higher the accuracy of the obtained MC results and also the higher the execution time needed by the MC algorithm. The MC results which will be presented in Section 5 have been obtained by adopting $N_{trials} = 10^6$. Such a value of N_{trials} has been chosen as a result of a reasonable trade-off between accuracy of results and duration of the execution time. By means of a very high number of tests it has been verified that, in the considered case ($N_{PV} = 24$, SP architecture, two strings), the improvement obtained by increasing N_{trials} above 10^6 is negligible, from the practical point of view. So that it is not necessary at all to further increase the number of MC trials. Nevertheless N_{trials} is about four order of magnitude higher than the typical number N_{SUBSET} of configurations which need to be analyzed by the proposed algorithm. As a consequence, as it has been verified by monitoring the execution times of the algorithms running in MATLAB, also the ratio between the execution time of the MC search and the execution time of the proposed algorithm is equal to about 10^4.

4. Experimental results

We explicitly remark here that the *I–V* modules characteristics of the various cases which will be discussed in the following are actual experimental characteristics. Instead, the *I–V* characteristics of the arrays resulting from the parallel connection of the two strings which can be obtained by means of different allocations of the 24 PV modules have been numerically obtained as discussed in Section 3 (Step 4). The *I–V* modules characteristics have been detected by means of proper measuring systems applied to the modules of a real PV field. With obvious meaning of the adopted symbols the salient parameters of the considered PV modules in STC are: $I_{SC} = 8.62$ A; $V_{OC} = 37.3$ V; $V_{MPP} = 30.7$ V; $P_{MPP} = 245$ W; $I_{MPP} = 7.99$ A; NOCT = 44 °C. The Geographic coordinates of the installation site are: Latitude: 41°04′59″N; Longitude: 14°20′05″E. The installation angles of the 24 PV modules of the array are: Azimuth angle: 72° (South–West); Tilt angle: 8°. In Fig. 1(a) a bird's-eye view of the considered PV field is provided. While in Fig. 1(b) some sources of shadows on the plant are evidenced by means of red circles (chimney and street lighting) and by means

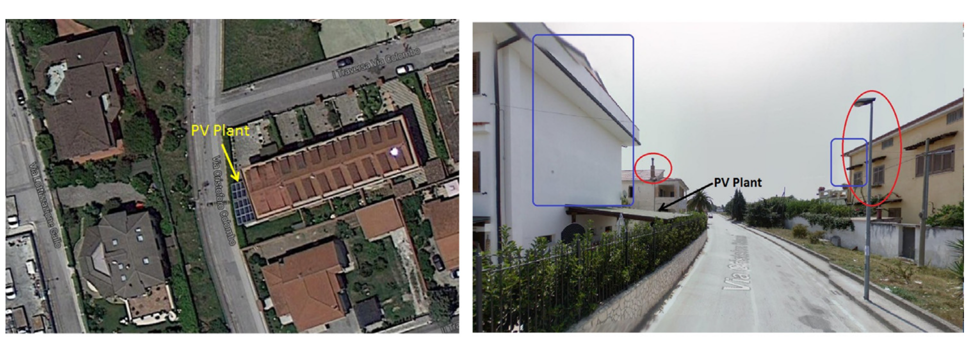

(a) (b)

Fig. 1. (a) Bird's-eye view of the PV field; (b) Sources of shadowing.

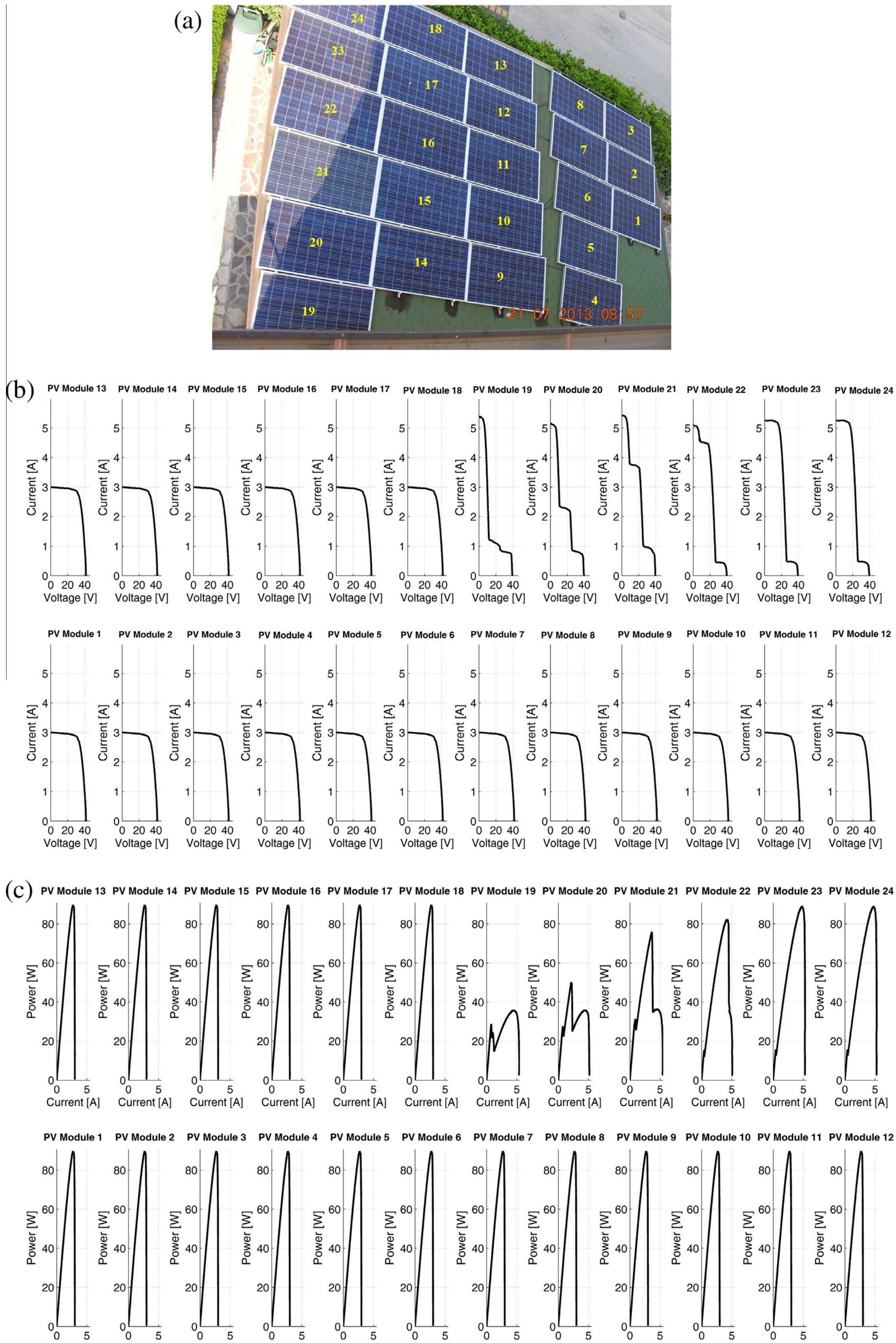

Fig. 2. (a) Picture of the PV field, Case 1; (b) *I–V* characteristics of the 24 PV modules, Case 1; (c) *P–I* characteristics of the 24 PV modules, Case 1.

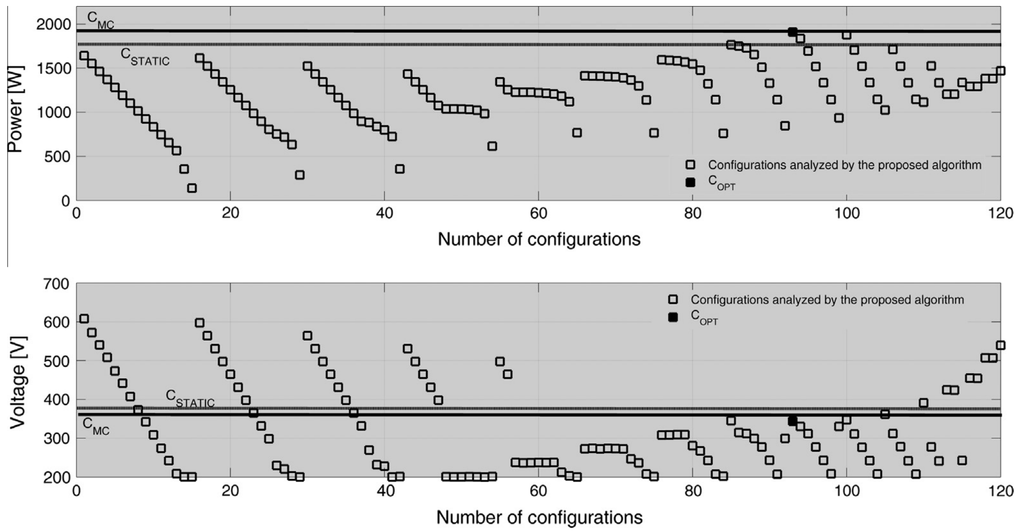

Fig. 3. Maximum powers of the analyzed configurations (upper subplot) and corresponding operating voltages (lower subplot), Case 1.

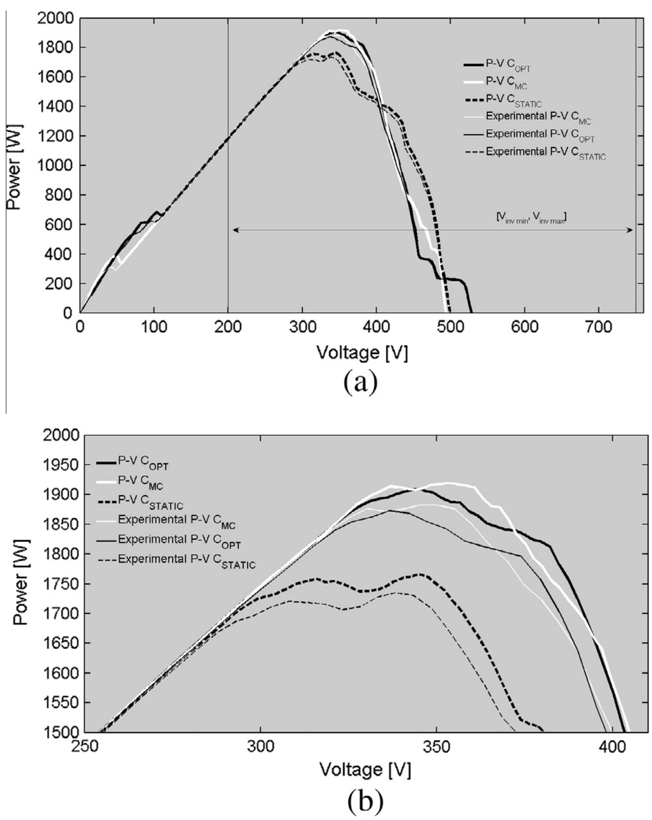

Fig. 4. (a) *P–V* curves, Case 1; (b) zoom of (a).

of blue rectangles (small wall and neighboring building). It is worth noting that the PV plant of Fig. 1(a) is a real residential plant. As it will be evident from the following analysis, its installation has not been optimized at all and, during the day, a number of shadowing phenomena occur. Such a PV field has been chosen since, due to the mismatching drawbacks it suffers during its operation, it allows to put in evidence a number of interesting aspects. Very often in the recent past, at least in Italy, the existence of generous feed-in tariffs and the corresponding stringent deadlines have encouraged the installation of non-optimized PV plants like the one under consideration.

In the following, four specific cases will be analyzed in detail.

4.1. Case 1

The first case takes place in the morning (8.57 AM, 21 July 2013). As it is evident from Fig. 2(a), apart from 6 PV modules (Modules 19, 20, ..., 24) which are partially shaded, the remaining 18 PV modules are fully shaded. The *I–V* characteristics of the 24 PV modules are shown in Fig. 2(b). The *P–I* characteristics are shown instead in Fig. 2(c). As expected, the curves of the fully shaded PV modules are nearly equal and exhibit the standard shape with a single MPP. The partially shaded modules instead exhibit the presence of two or even three maxima.

The number of configurations which is analyzed by the proposed algorithm is $N_{SUBSET} = 120$, since $N_{MIN} = 5$ ($V_{inv\_min}/V_{oc\_max} = 200\text{ V}/39.21\text{ V} = 5.1$) and $N_{MAX} = 19$ ($V_{inv\_max}/V_{oc\_min} = 750\text{ V}/38.86\text{ V} = 19.3$). In the considered case it is $b = 4$. In Fig. 3 (upper subplot) the maximum power which can be obtained by adopting each of such 120 analyzed configurations is indicated by means of an empty square marker. The white filled square marker indicates the maximum power which can be obtained by adopting the configuration associated to C_{OPT}. In the considered case it is $C_{OPT} = [1\,1\,1\,1\,1\,1\,1\,2\,2\,2\,2\,2\,2\,2\,2\,2\,2\,2\,1\,1\,1\,1\,1\,1]$.

Therefore no PV module has been discarded. The configuration vector of the best MC configuration will be indicated with the symbol C_{MC}. In the considered case it is $C_{MC} = [1\,2\,2\,2\,2\,2\,1\,1\,2\,1\,2\,1\,1\,2\,1\,2\,1\,1\,2\,1\,2\,2\,1\,1]$. The thick horizontal line in Fig. 3 (upper subplot) just represents the maximum power level which can be obtained by adopting the configuration associated to C_{MC}. The configuration vector of the static configuration will be indicated with the symbol C_{STATIC}; it is $C_{STATIC} = [1\,1\,1\,1\,1\,1\,1\,1\,1\,1\,1\,1\,2\,2\,2\,2\,2\,2\,2\,2\,2\,2\,2\,2]$. The dashed horizontal line in Fig. 3 (upper subplot) just represents the maximum power level which can be obtained by adopting the configuration associated to C_{STATIC}. In Fig. 3 (lower subplot), with the same meaning of the adopted symbols, the MPP voltages of the various analyzed configurations are reported.

From the analysis of Fig. 3 it is evident that, although C_{OPT} is quite different from C_{MC}, the corresponding maximum powers are nearly equal. In particular, the *P–V* curves associated to C_{OPT}, C_{MC} and C_{STATIC} are shown in Fig. 4(a). It is worth noting that, in Fig. 4(a), not only the *P–V* curves which have been numerically obtained as explained in Section 3 (Step 4), but also the corresponding experimental *P–V* curves have been reported. Fig. 4(b) shows a zoom of Fig. 4(a).

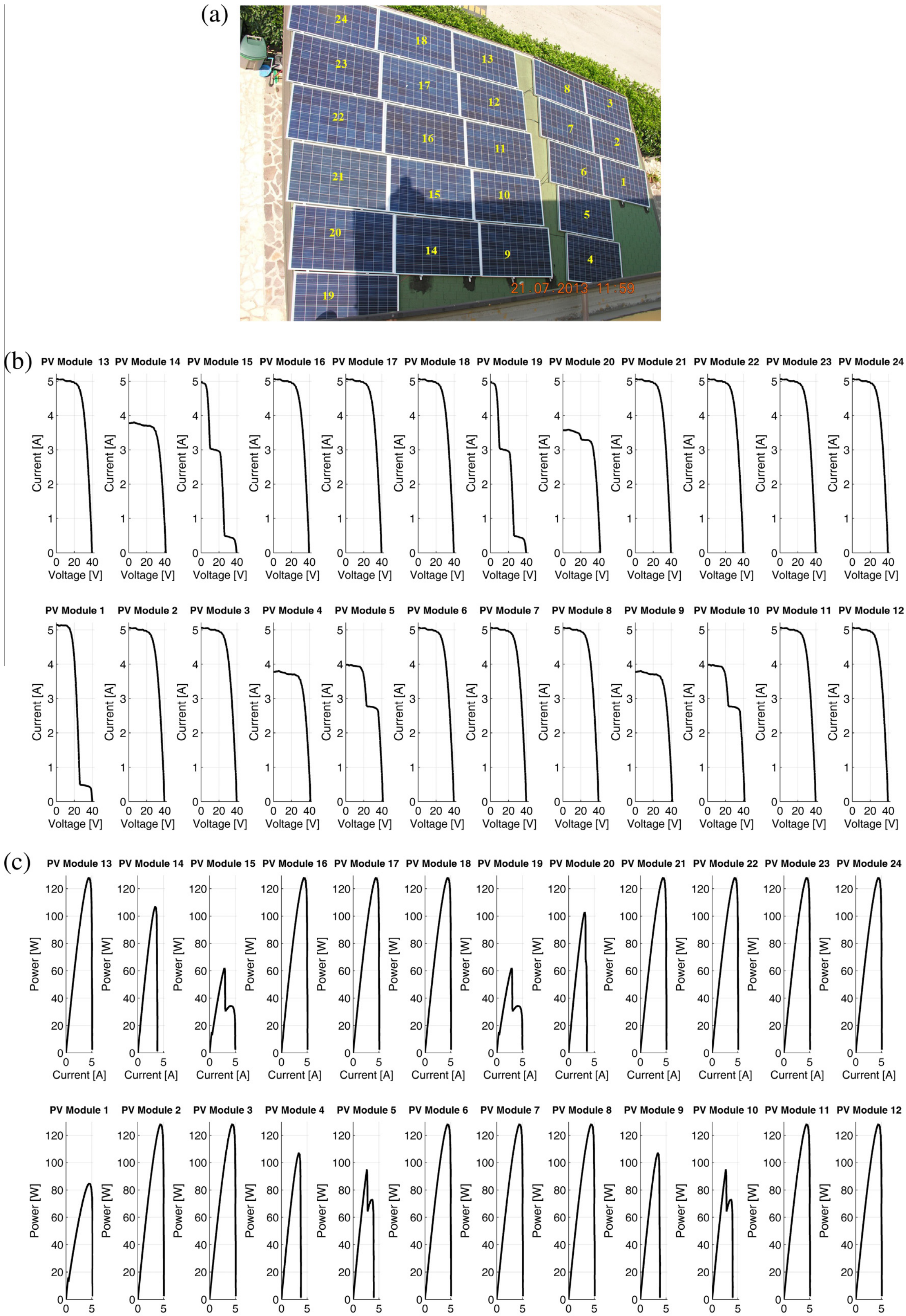

Fig. 5. (a) Picture of the PV field, Case 2; (b) *I–V* characteristics of the 24 PV modules, Case 2; (c) *P–I* characteristics of the 24 PV modules, Case 2.

With reference to the *P–V* curves which have been numerically obtained, the maximum power P_{CMC} associated to C_{MC} is equal to 1920 W, the maximum power P_{COPT} associated to C_{OPT} is equal to 1910 W, while the maximum power P_{STATIC} associated to C_{STATIC} is equal to 1766 W. The sum P_{TOT} of the maximum powers of the 24 PV modules is instead equal to about 2036 W.

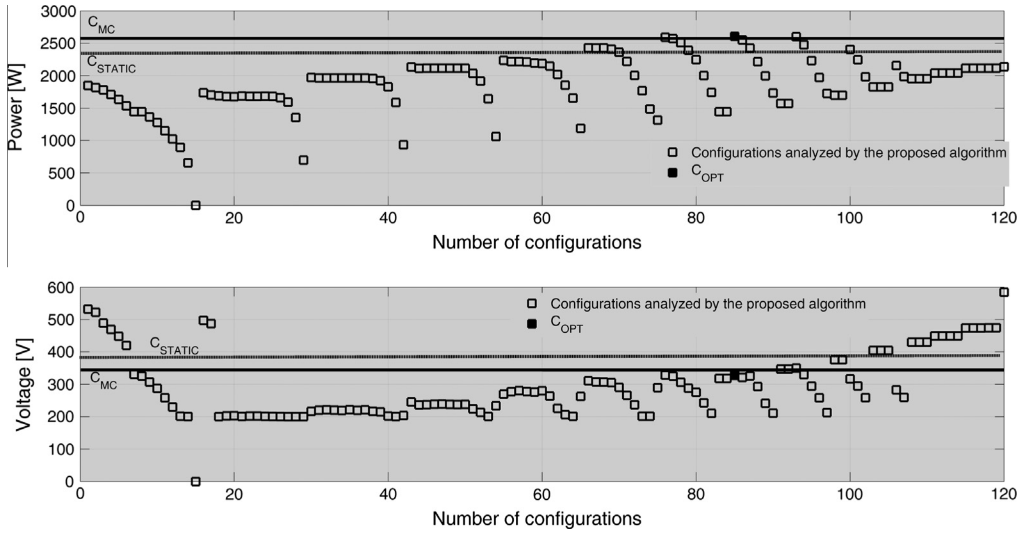

Fig. 6. Maximum powers of the analyzed configurations (upper subplot) and corresponding operating voltages (lower subplot), Case 2.

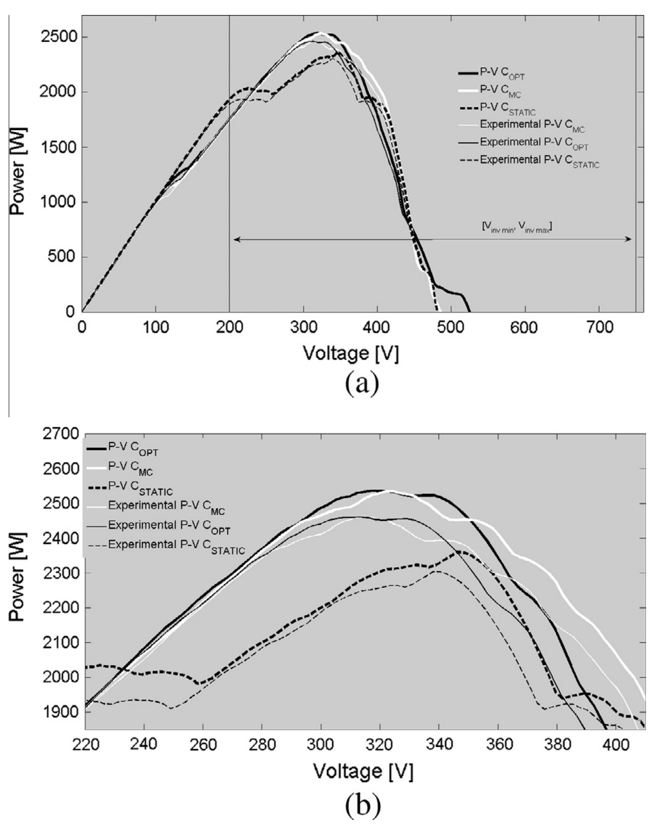

Fig. 7. (a) *P–V* curves, Case 2; (b) zoom of (a).

Instead, with reference to the experimental *P–V* curves, the maximum power P_{CMC_EXP} associated to C_{MC} is equal to 1882 W, the maximum power P_{COPT_EXP} associated to C_{OPT} is equal to 1873 W, while the maximum power P_{STATIC_EXP} associated to C_{STATIC} is equal to 1735 W. Although the unavoidable differences among numerical and corresponding experimental values, the main result which is worth noting here is that both numerical and fully experimental results indicate that the highest maximum power is that one associated to C_{MC} and that such a power is only slightly higher than the maximum power associated to C_{OPT}. Similar considerations also hold for the other Cases which are discussed in the following and, for the sake of brevity, they will not be repeated.

In order to quantify the performances of the various configurations, let's define the following efficiencies:

$$\eta_{STATIC} = (P_{STATIC\_EXP}/P_{TOT}) \cdot 100\% \tag{5}$$

$$\eta_{COPT} = (P_{COPT\_EXP}/P_{TOT}) \cdot 100\% \tag{6}$$

$$\eta_{CMC} = (P_{CMC\_EXP}/P_{TOT}) \cdot 100\% \tag{7}$$

In Case 1 we get η_{STATIC} = 85.22%, η_{COPT} = 92%, η_{CMC} = 92.44%. Therefore the proposed algorithm is able to quickly lead to an increase of the efficiency, with respect to the static configuration, of about 6.78%; while the MC search is able to lead to an increase of the efficiency of about 7.22%, but only after an unfeasible number of calculations (10^6 trials).

4.2. Case 2

Case 2 takes place in the morning (11.50 AM, 21 July 2013). A picture of the shaded field is shown in Fig. 5(a). The *I–V* characteristics of the 24 PV modules are shown in Fig. 5(b). The *P–I* characteristics are shown in Fig. 5(c). In Fig. 6 (upper subplot), with the same symbols adopted before, the maximum powers which can be obtained by adopting the various analyzed configurations are indicated. In the considered case it is C_{OPT} = [2 1 1 2 2 1 1 1 2 2 1 1 2 2 2 2 2 2 2 2 1 1 1 1]. Therefore, also in this case, no PV module has been discarded. It is also C_{MC} = [2 2 2 1 1 2 2 2 1 1 1 2 2 1 1 1 2 2 1 1 1 2 2 2]. In Fig. 6 (lower subplot), the MPP voltages of the various analyzed configurations are reported.

The *P–V* numerical and experimental curves which concern Case 2 and which are associated to the corresponding configuration vectors C_{OPT}, C_{MC} and C_{STATIC} are shown in Fig. 7(a). Fig. 7(b) shows a zoom of Fig. 7(a).

In Case 2, it is P_{CMC} = 2535 W, P_{COPT} = 2537 W, P_{STATIC} = 2360 W, P_{CMC_EXP} = 2462 W; P_{COPT_EXP} = 2463 W and P_{STATIC_EXP} = 2304 W. The sum P_{TOT} of the maximum powers of the 24 PV modules is instead equal to about 2709 W.

Therefore, it is η_{STATIC} = 85.1%, η_{COPT} = 90.9%, η_{CMC} = 90.8%. Hence the proposed algorithm is able to quickly lead to an increase of the efficiency of about 5.8%, while the MC search, although the considerably higher number of calculations, is able to lead to a nearly equal increase of the efficiency (5.7%).

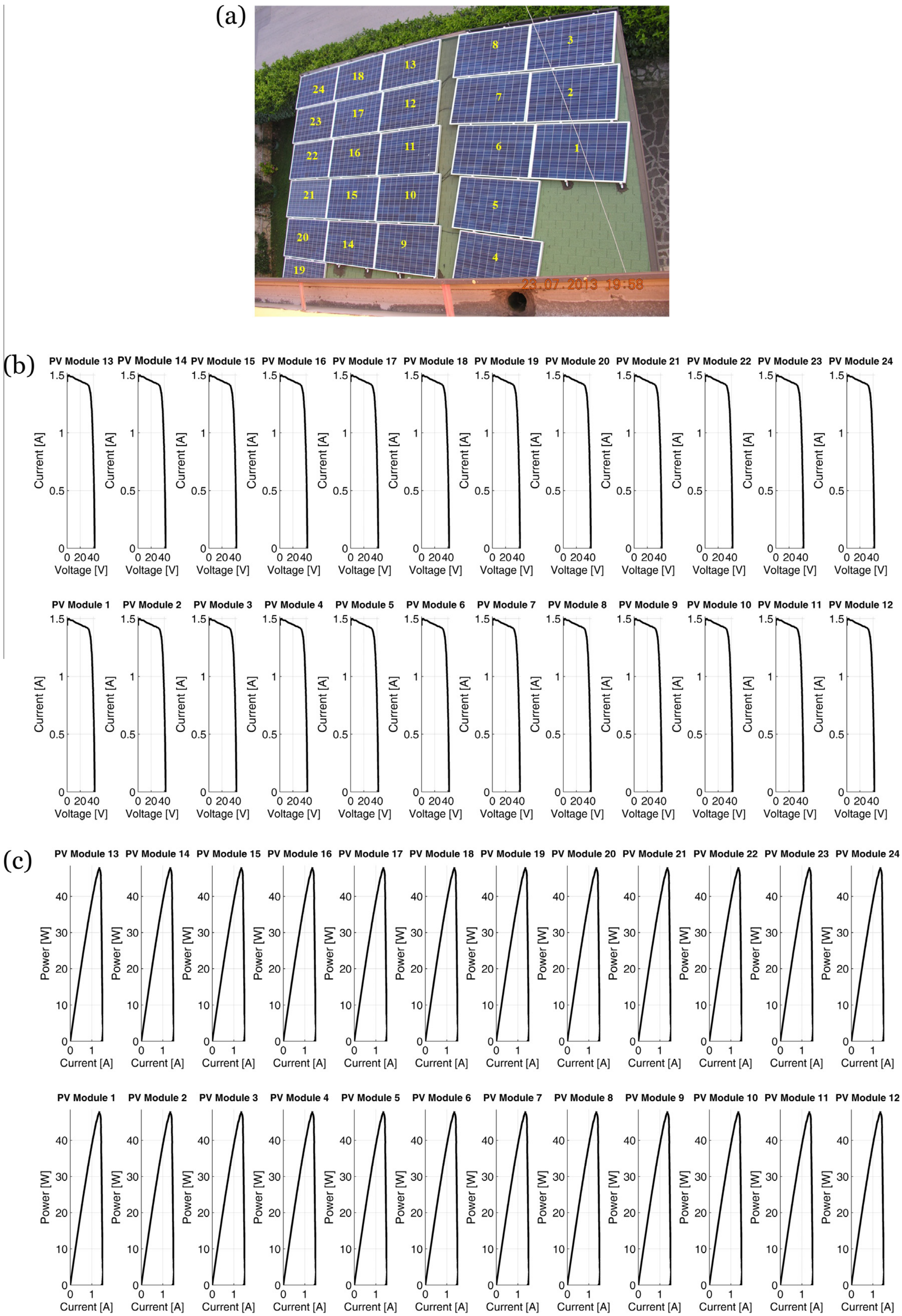

Fig. 8. (a) Picture of the PV field, Case 3; (b) *I–V* characteristics of the 24 PV modules, Case 3; (c) *P–I* characteristics of the 24 PV modules, Case 3.

4.3. Case 3

Case 3 takes place in the evening (19.58 PM, 23 July 2013). A picture of the uniformly irradiated PV field is shown in Fig. 8(a). The *I–V* characteristics of the 24 PV modules are shown in Fig. 8 (b). Such characteristics are not perfectly equal due to uneven aging, manufacturing tolerances, measuring errors, etc. The values of the short circuit currents in Fig. 8(b) clearly indicate that the sunset is approaching and the value of the irradiation is quite low.

In the considered case it is C_{OPT} = [1 1 1 1 1 1 1 1 1 1 1 1 2 2 2 2 2 2 2 2 2 2 2 2]. Therefore, also in this case, no PV module has been discarded by the proposed algorithm. It is also C_{MC} = [2 2 2 2 1 1 1 2 1 1 1 1 2 2 2 1 2 2 2 1 1 1 2 1]. It is worth noting that, although at a first sight it seems that C_{OPT} is completely different from C_{MC}, indeed the two configurations vectors are nearly equivalent since, as evidenced above, the *I–V* characteristics of the 24 PV modules are nearly equal. Only the unavoidable small differences among such *I–V* characteristics justify the apparently random allocation of the 24 PV modules among the two strings in C_{MC}. Such considerations are confirmed by Fig. 9 where the numerical and experimental *P–V* curves associated to C_{OPT}, C_{MC} and C_{STATIC} are nearly superimposed. For the sake of completeness, in Case 3 we get P_{CMC} = 1145 W; P_{COPT} = 1145 W; P_{STATIC} = 1145 W; $P_{CMC-EXP}$ = 1136 W; P_{COPT_EXP} = 1136 W; P_{STATIC_EXP} = 1136 W. In a case like this, re-configuration is useless; rather it is counterproductive if the waste of power which necessary to the commutations, taking place during the interval of time needed for the measurement of the *I–V* characteristics of the PV modules, is taken into account. Indeed, the discussion of Case 3 has been provided just in order to stress such an important advantage of re-configuration systems with respect to DMPPT systems. As discussed in the introduction of the paper, during the more or less prolonged periods of time which are characterized by uniform atmospheric conditions (like in Case 3), the re-configuration systems do not waste additional power since no commutation of the switches is required. The absence of commutations is guaranteed by the equality $C_{OPT} = C_{STATIC}$ which has been obtained in Case 3. Instead, in a DMPPT systems, even under uniform atmospheric conditions, the dc/dc converters would be forced to process anyhow the PV power thus leading to unavoidable additional power losses.

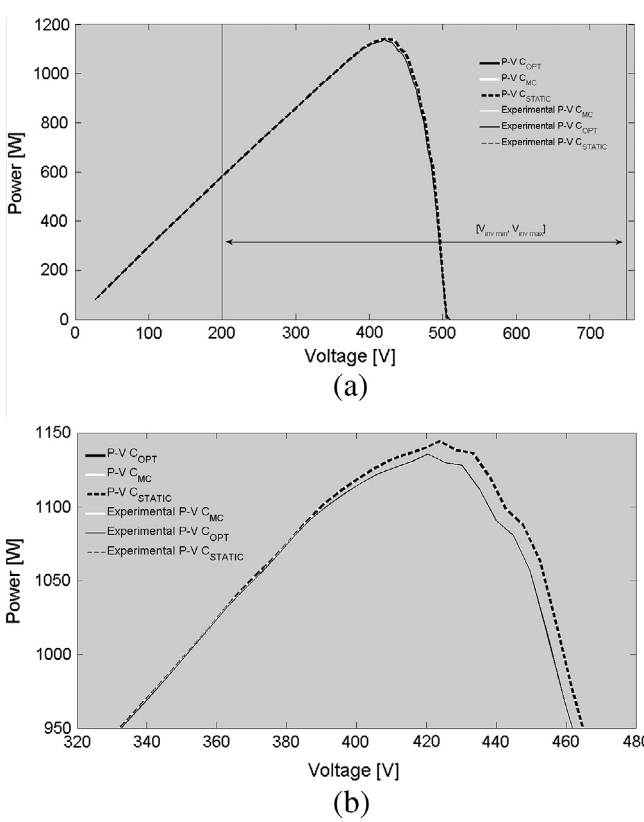

Fig. 9. (a) *P–V* curves, Case 3; (b) zoom of (a).

4.4. Case 4

Case 4 takes place in the evening (18.50 PM, 23 July 2013). A picture of the PV field in Case 4 is shown in Fig. 10(a) where the shadow caused by a neighboring pole is particularly evident. The *I–V* characteristics of the 24 PV modules are shown in Fig. 10(b). The corresponding *P–I* characteristics are shown in Fig. 10(c).

In such a case it is C_{OPT} = [1 1 2 1 1 1 1 1 2 1 1 1 2 2 1 2 2 2 2 2 2 2 2 2] and C_{MC} = [2 2 2 2 1 1 1 2 1 1 1 1 2 2 2 1 2 2 2 1 1 1 2 1]. In Case 4, it is P_{CMC} = 884 W, P_{COPT} = 884 W, P_{STATIC} = 816.8 W, P_{TOT} 1114 W, P_{CMC_EXP} = 867 W, $P_{COPT-EXP}$ = 869 W and $P_{STATIC-EXP}$ = 805 W (see Fig. 11). Therefore, it is η_{STATIC} = 72.3%, η_{COPT} = 78%, η_{CMC} = 77.8%. In conclusion, in the above cases (and in all the other ones which have been examined but have not been reported here for the sake of brevity) the proposed algorithm is able to find a suboptimal solution with a very limited computational burden if compared to the MC based algorithm. The comparison among experimental and numerical results allows to confirm that there is no need to experimentally detect the *P–V* characteristics associated to the various analyzed configurations. Much more easily, such characteristics can be instead numerically obtained from the experimental characteristics of the single PV modules. This is enough for the correct and robust working of the proposed algorithm and it is a crucial aspect which is worth noting. In fact, the practical implementation of the proposed algorithm only requires the knowledge of the experimental curves of the single PV modules. Instead, the experimental *P–V* characteristics of the various analyzed configurations are not required at all by the proposed method. This is highly desirable since it would be unpractical and inadvisable, if not impossible, to get them during the normal working of the dynamic re-configuration algorithm. In fact, apart from the unacceptable long time required to set the analyzed array configurations and to get the corresponding experimental characteristics, another important aspect to take into account is also the minimization of the number of commutations of the switches, in order to avoid their premature failure or accelerated aging. The proposed method, on the basis of *I–V* or *P–V* array characteristics which need to be only numerically (and not experimentally) evaluated, is able to identify a nearly optimal configuration. The final (ON or OFF) states of the switches are set only after that such an optimal configuration has been found.

5. Re-configuration as mean to limit premature aging

In this section it will be shown that the PV modules connections can be re-configured in such a way that it is possible, not only to extract higher energy with respect to the case of a static architecture, but also to prevent the occurrence of phenomena leading to the premature aging or even to the failure of one or more PV modules of the array. We explicitly remark here that only some preliminary, basic considerations will be discussed in this section. The whole topic deserves major attention and will be the subject of forthcoming papers. The starting point is represented by the analysis of the shape of the *I–V* characteristic of a string of PV modules. It is well known that, if such a characteristic contains more than one knee, then, depending on the value of the string current, one

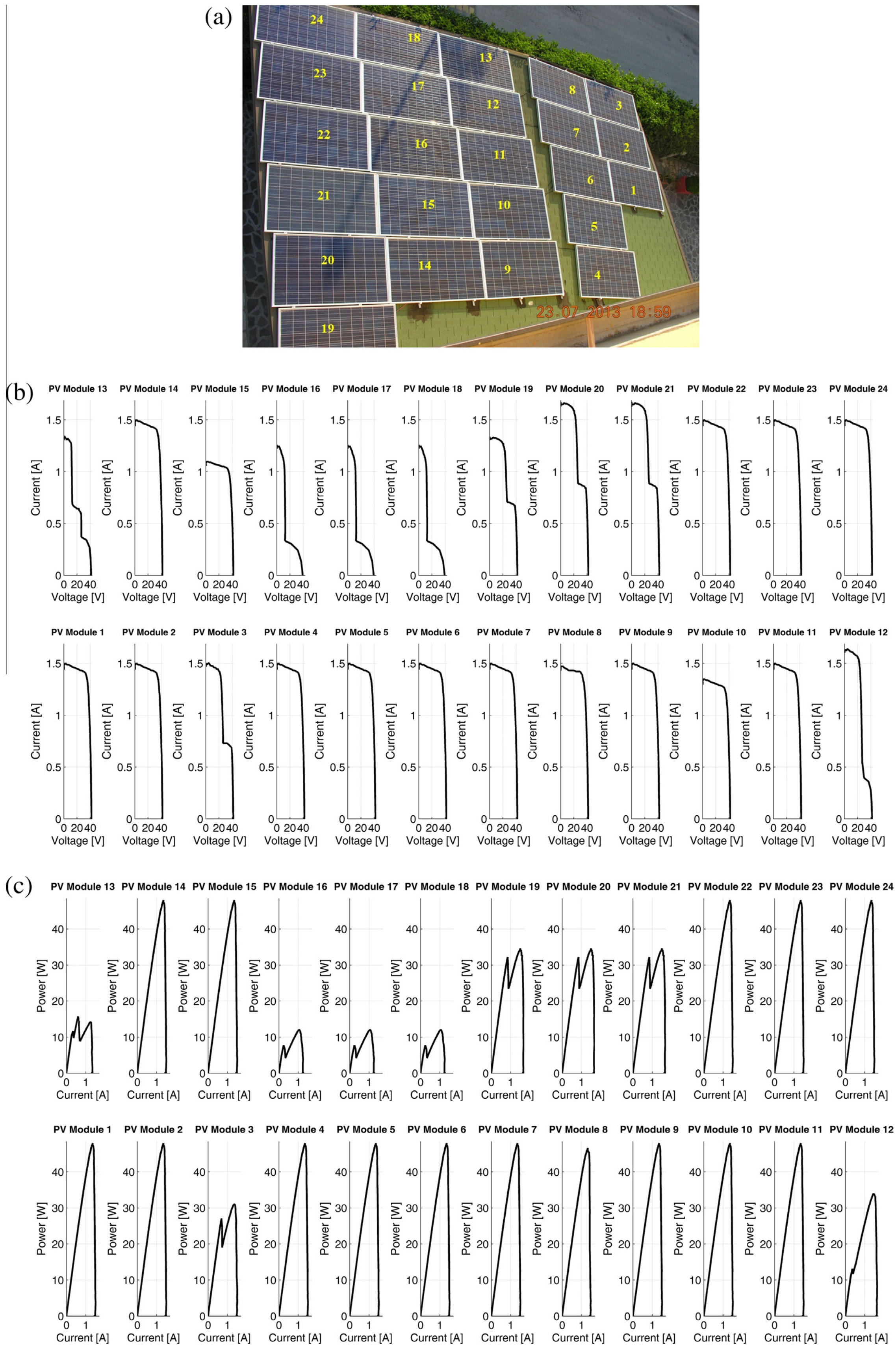

Fig. 10. (a) Picture of the PV field, Case 4; (b) *I–V* characteristics of the 24 PV modules, Case 4; (c) *P–I* characteristics of the 24 PV modules, Case 4.

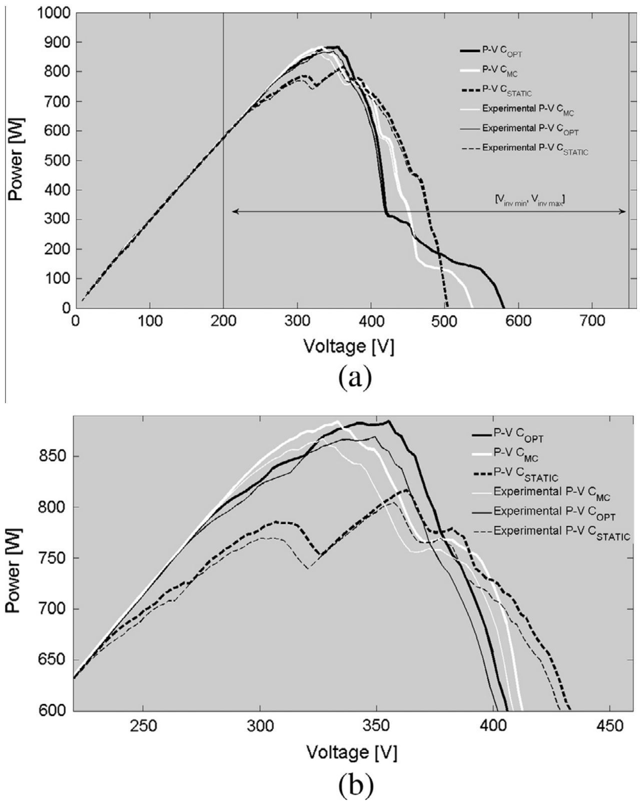

Fig. 11. (a) P–V curves, Case 4; (b) zoom of (a).

or more by-pass diodes can conduct currents and/or one or more cells or string of cells can be reverse biased. The by-pass diodes conduction (especially for prolonged times) and/or the reverse biasing of the PV cells represent dangerous operating conditions since they may lead to the premature aging and to the failures of the PV modules due to enhanced thermal stresses [55–58]. It is therefore highly desirable to avoid the occurrence of the above dangerous operating conditions. In order to completely avoid by-pass diodes conduction and cells reverse biasing it is necessary to limit the string current below the lowest current value among the current values characterizing the knees of the I–V string characteristic. Let's consider once again the Case 2 which has been analyzed before. In Fig. 12 (left subplot) the I–V characteristics of the 11 modules which, in order to maximize the extraction of energy, should be placed in the String 1 according to C_{OPT} are shown. Instead, in the right subplot of Fig. 12, the I–V characteristics of the 13 remaining modules which, always according to C_{OPT}, should be placed in the String 2 are shown. The horizontal dashed lines represent the values of the operating currents flowing in the two strings when the whole PV array operates at its MPP ($I_{string\ 1} = I_{string\ 1\ MPP}$, $I_{string\ 2} = I_{string\ 2\ MPP}$). Of course, in general, such operating currents are different. It is evident that, in the case of the String 2, the corresponding operating current $I_{string\ 2\ MPP}$ is higher than one or more knees of the I–V characteristics of the following PV modules (which have been assigned just to String 2 by the proposed algorithm): 1, 5, 10, 15, 19 and 20. As concerns instead the String 1, its PV modules exhibit only one peak in their P–I characteristics and hence no dangerous operating condition can occur whichever the value of $I_{string\ 1}$. Summarizing, the solution provided by C_{OPT} is not suitable to avoid the occurrence of dangerous operating conditions. In fact, in order to avoid such conditions, the operating voltage of the String 2 (and hence that one of the String 1 which is in parallel) should be increased in order to decrease the value of $I_{string\ 2}$ from $I_{string\ 2\ MPP}$ ($I_{string\ 2\ MPP} = 3.3$ A) to $I^*_{string\ 2}$ ($I^*_{string\ 2} = 0.42$ A). As shown in Fig. 12, $I^*_{string\ 2}$ represents the lowest knee current of PV modules 15 and 19. As a consequence, as shown in Fig. 13 where the P–V characteristics of the two strings are reported, the power drawn from String 1 and from String 2 would become unacceptably low. Indeed, according to Fig. 13, String 1 would operate in open circuit conditions.

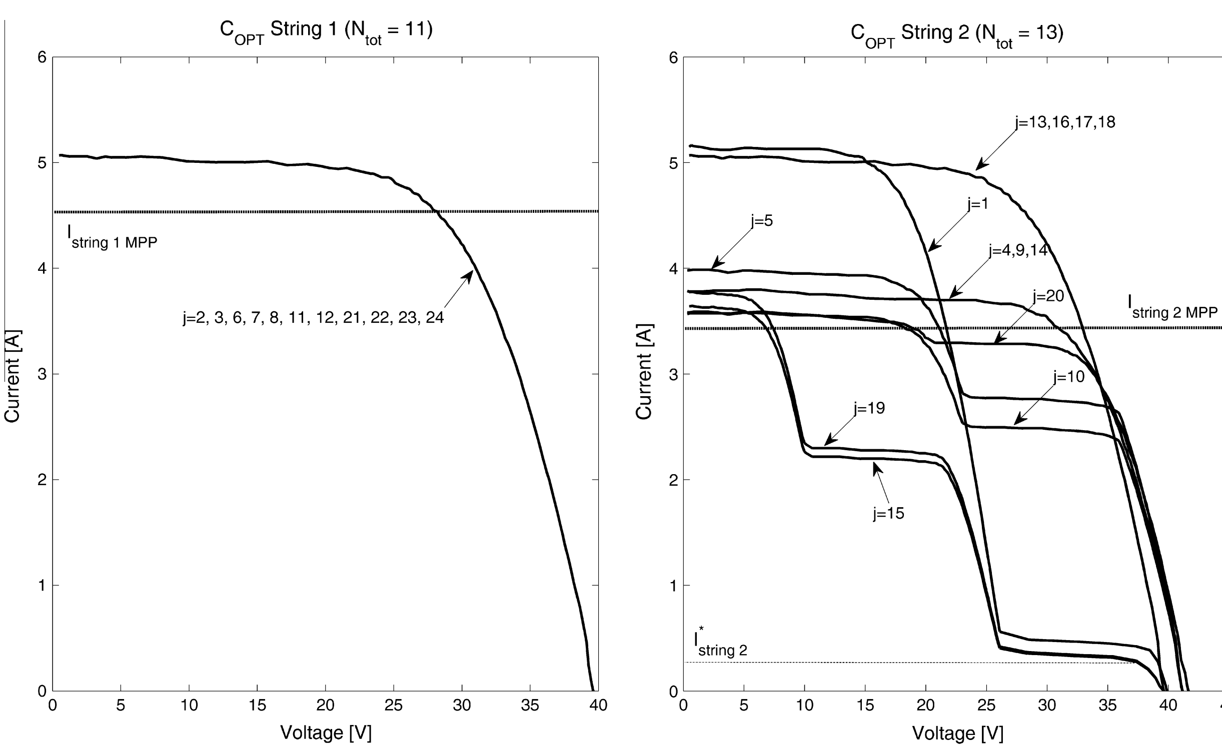

Fig. 12. I–V curves of modules belonging to String 1 (left figure) and to String 2 (right figure), Case 2, C_{OPT}.

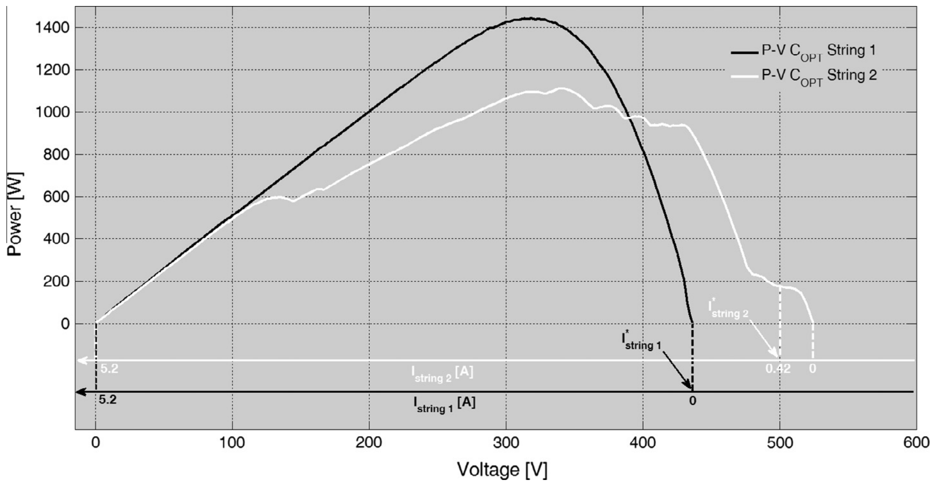

Fig. 13. *P–V* curves of Strings 1 and 2, Case 2, C_{OPT}.

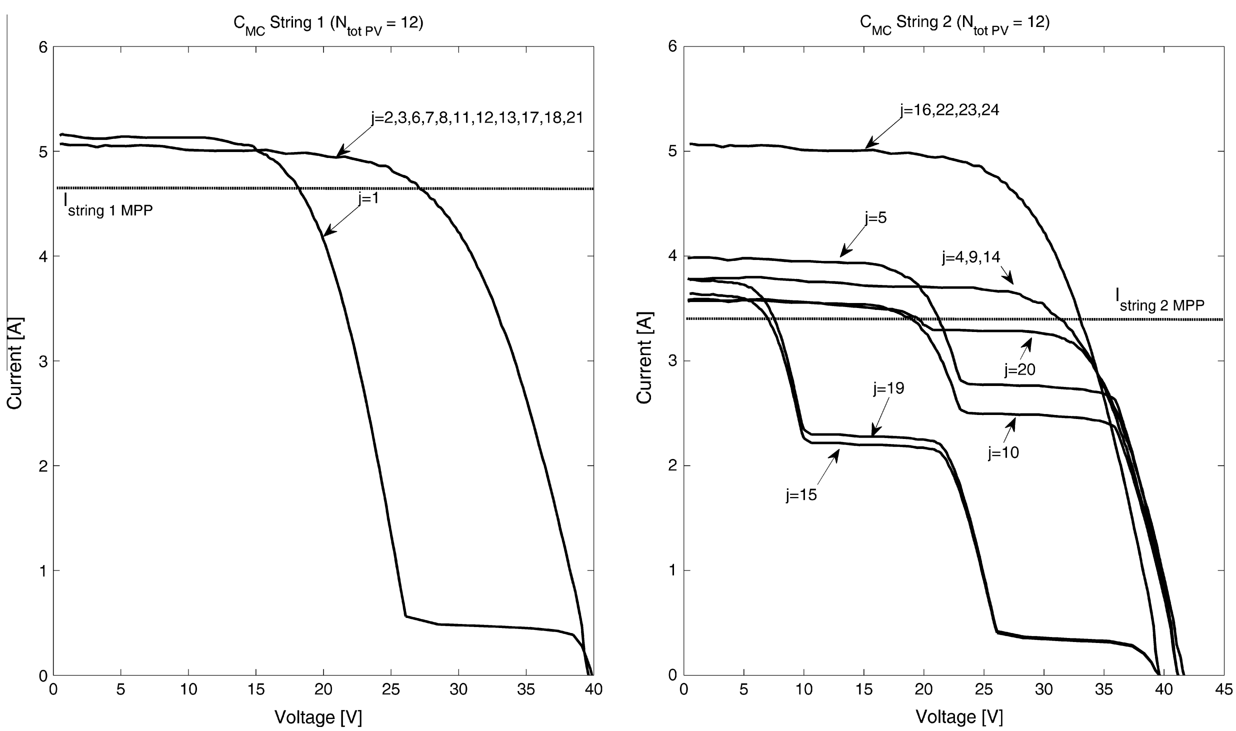

Fig. 14. *I–V* curves of modules belonging to String 1 (left figure) and to String 2 (right figure), Case 2, C_{MC}.

The situation is even worse if the solutions associated to C_{MC} (Fig. 14) and to C_{STATIC} (Fig. 15) are analyzed. In such cases in fact, the operating condition is dangerous also for some modules belonging to String 1.

On the basis of the above considerations, it is clear that, even if all the re-configuration algorithms which have been presented so far in the literature, including the one proposed in this paper, are focused on the maximization of the extracted energy, indeed the need exists for algorithms which are capable of providing configurations which are able to prevent the occurrence of premature aging or failures of the PV modules. Nearly always maximization of energy and absence of dangerous operating conditions are contrasting requirements. Anyway, it is possible to find configurations which represent a suitable compromise between such contrasting requirements. As an example, among the various configurations analyzed by the MC algorithm in Case 2, the one associated to the configuration vector C^* is worth to be analyzed. In particular it is $C^* = [0\,1\,1\,2\,2\,1\,1\,1\,2\,2\,1\,1\,2\,2\,0\,2\,2\,2\,0\,2\,1\,1\,1\,1]$. In such a case, 3 PV modules have been discarded. In Fig. 16 (left subplot) the *I–V* characteristics of the modules which, according to C^*, should be placed in the String 1 are shown. Instead, in the right subplot of Fig. 16, the *I–V* characteristics of the remaining modules to be placed in the String 2 are reported. It is evident that, by adopting the configuration vector C^*, no dangerous operating condition occurs at the MPP. In Fig. 17 the *P–V* curves concerning Case 2 are reported. By adopting C^*, the obtained efficiency is $\eta^* = 89.43\%$. Therefore, although providing more than 2% gain of efficiency with respect to C_{STATIC}, C^* is also able to avoid body diodes conduction or reverse biasing of cells.

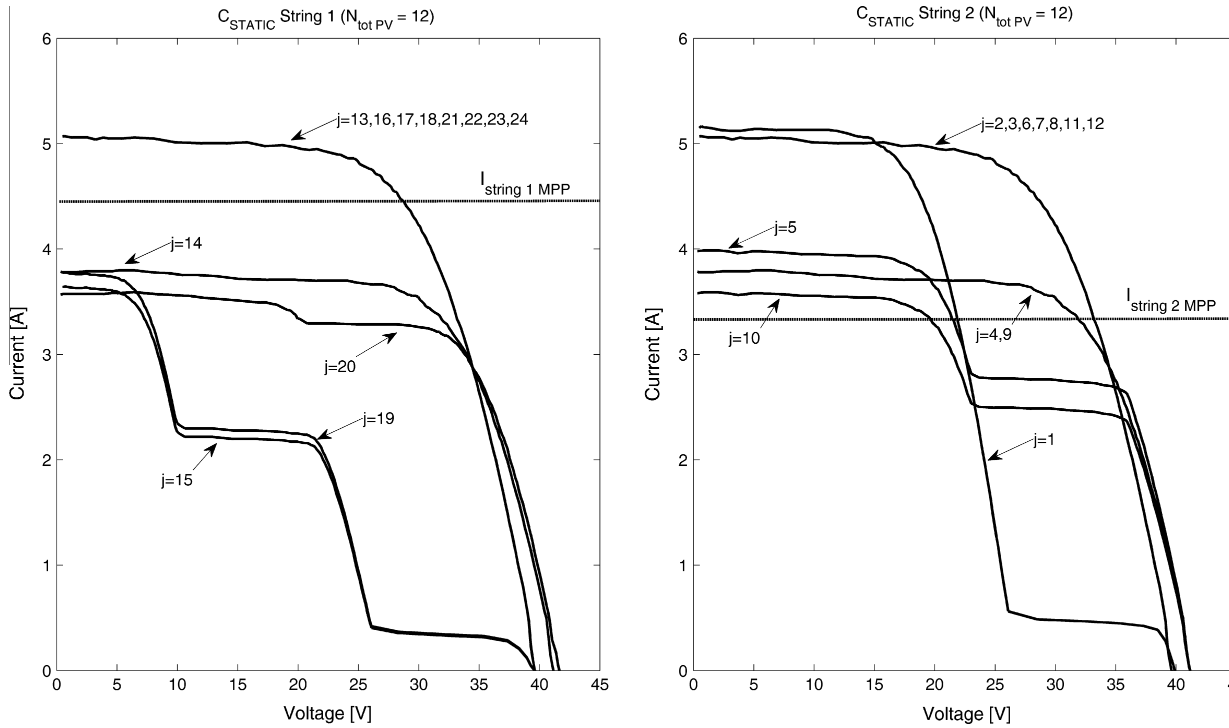

Fig. 15. *I–V* curves of modules belonging to String 1 (left figure) and to String 2 (right figure), Case 2, C_{STATIC}.

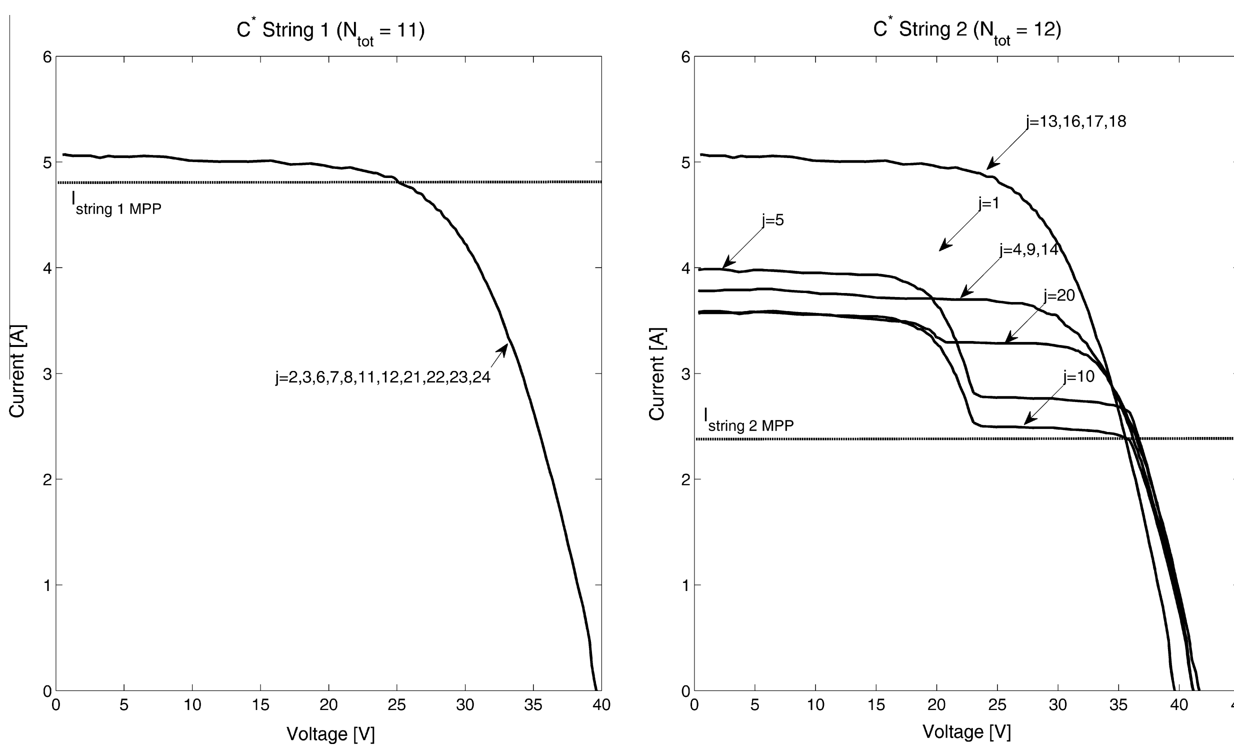

Fig. 16. *I–V* curves of modules belonging to String 1 (left figure) and to String 2 (right figure), Case 2, C^{*}.

6. Conclusions

In this paper a simple and quick algorithm leading to the identification of a suboptimal reconfiguration of a PV array with a SP architecture has been presented and discussed. It has been shown that, in real-life mismatching operating conditions of an actual PV array composed by 24 PV modules, the algorithm is able to provide performances which are more or less comparable with those ones provided by a MC based algorithm employing a much higher number of trials. By means of a specific example, it has been also shown that maximization of extracted energy and absence of dangerous operating conditions, leading to premature aging of the PV field and/or to hot spot phenomena, are contrasting requirements. Nevertheless it is possible to find proper configurations able to lead to a suitable compromise between such contrasting requirements. Further work is needed and is in progress in order to design

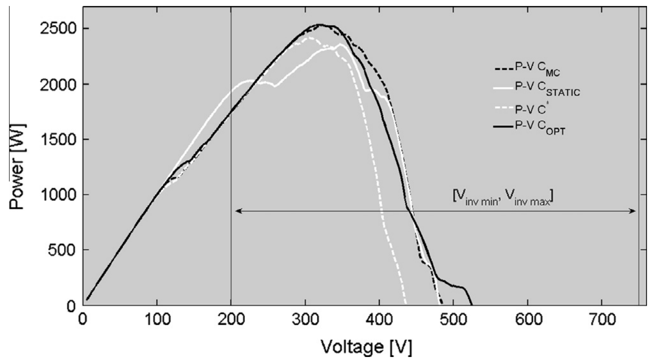

Fig. 17. *P–V* curves Case 2.

suitable re-configuration algorithms able to identify such compromise configurations.

References

[1] Reinoso CRS, Milone DH, Buitrago RH. Simulation of photovoltaic centrals with dynamic shading. Appl Energy 2013;103(March):278–89.

[2] Said SAM. Effects of dust accumulation on performances of thermal and photovoltaic flat-plate collectors. Appl Energy 1990;37(1):73–84.

[3] Agrawal B, Tiwari GN. Optimizing the energy and exergy of building integrated photovoltaic thermal (BIPVT) systems under cold climatic conditions. Appl Energy 2010;87(2):417–26.

[4] Sun L, Lu L, Yang H. Optimum design of shading-type building-integrated photovoltaic claddings with different surface azimuth angles. Appl Energy 2012;90(1):233–40. ISSN 0306-2619.

[5] Eke R, Senturk A. Monitoring the performance of single and triple junction amorphous silicon modules in two building integrated photovoltaic (BIPV) installations. Appl Energy 2013;109(September):154–62.

[6] Mulcué-Nieto LF, Mora-López L. Methodology to establish the permitted maximum losses due to shading and orientation in photovoltaic applications in buildings. Appl Energy 2015;137(1):37–45.

[7] Cuce E, Cuce PM, Bali T. An experimental analysis of illumination intensity and temperature dependency of photovoltaic cell parameters. Appl Energy 2013;111(November):374–82.

[8] Ahmed J, Salam Z. A maximum power point tracking (MPPT) for PV system using cuckoo search with partial shading capability. Appl Energy 2014;119(15):118–30.

[9] Lin CH, Huang CH, Du YC, Chen JL. Maximum photovoltaic power tracking for the PV array using the fractional-order incremental conductance method. Appl Energy 2011;88(12):4840–7.

[10] Jiang JA, Su YL, Shieh JC, Kuo KC, Lin TS, Lin TT, et al. On application of a new hybrid maximum power point tracking (MPPT) based photovoltaic system to the closed plant factory. Appl Energy 2014;124(1):309–24.

[11] Kumar G, Trivedi MB, Panchal AK. Innovative and precise MPP estimation using P–V curve geometry for photovoltaics. Appl Energy 2015;138(15):640–7.

[12] Kumar G, Panchal AK. Geometrical prediction of maximum power point for photovoltaics. Appl Energy 2014;119(15):237–45.

[13] Salam Z, Ahmed J, Merugu BS. The application of soft computing methods for MPPT of PV system: a technological and status review. Appl Energy 2013;107(July):135–48.

[14] Femia N, Petrone G, Spagnuolo G, Vitelli M. Optimization of perturb and observe maximum power point tracking method. IEEE Trans Power Electron 2005;20(4):963–73.

[15] Hohm DP, Ropp ME. Comparative study of maximum power point tracking algorithms. Prog Photovoltaics Res Appl 2003;11:47–62.

[16] Esram T, Chapman PL. Comparison of photovoltaic array maximum power point tracking techniques. IEEE Trans Energy Convers 2007;2:439–49.

[17] Femia N, Petrone G, Spagnuolo G, Vitelli M. A new analog MPPT technique: TEODI. Progr Photovolt: Res Appl 2010;18:28–41.

[18] Ishaque K, Salam Z, Lauss G. The performance of perturb and observe and incremental conductance maximum power point tracking method under dynamic weather conditions. Appl Energy 2014;119(15):228–36.

[19] Vitelli M. On the necessity of joint adoption of both distributed maximum power point tracking and central maximum power point tracking in PV systems. Progr Photovolt: Res Appl 2014;22:283–99.

[20] Walker GR, Sernia PC. Cascaded DC/DC converter connection of photovoltaic modules. IEEE Trans Power Electron 2004;19(July):1130–9.

[21] Femia N, Lisi G, Petrone G, Spagnuolo G, Vitelli M. Distributed maximum power point tracking of photovoltaic arrays: novel approach and system analysis. IEEE Trans Ind Electron 2008;55(July).

[22] Roman E, Alonso R, Ibanez P, Elorduizapatarietxe S, Goitia D. Intelligent PV module for grid-connected PV systems. IEEE Trans Ind Electron 2006;53(4):1066–73.

[23] Website: http://solarmagic.com/en/index.html.

[24] Website: http://www.solaredge.com.

[25] Website: http://www.tigoenergy.com.

[26] Website: http://www.xandex.com.

[27] Website: http://www.st.com.

[28] Website: http://eiqenergy.com.

[29] Kjaer SB, Pedersen JK, Blaabjerg F. A review of single-phase grid-connected inverters for photovoltaic modules. IEEE Trans Ind Appl 2005;41(5):1292–306.

[30] Li Quan, Wolfs P. A review of the single phase photovoltaic module integrated converter topologies with three different DC link configurations. IEEE Trans Power Electron 2008;23(3):1320–33.

[31] Website: http://www.enphaseenergy.com.

[32] Website: http://www.greenraysolar.com.

[33] Website: http://www.petrasolar.com.

[34] Website: http://www.enecsys.com.

[35] Website: http://www.exeltech.com.

[36] Website: http://solarbridgetech.com.

[37] Website: http://www.involar.com.

[38] Graditi G, Adinolfi G, Tina GM. Photovoltaic optimizer boost converters: temperature influence and electro-thermal design. Appl Energy 2014;115(15):140–50.

[39] Zhang P, Li W, Li S, Wang Y, Xiao W. Reliability assessment of photovoltaic power systems: review of current status and future perspectives. Appl Energy 2013;104:822–33.

[40] Faldella Eugenio, Cardinali Gian Carlo, Calzolari Pier Ugo. Architectural and design issues on optimal management of photovoltaic pumping systems. IEEE Trans Industr Electron 1991;38(5):385–92.

[41] Villa Luiz Fernando Lavado, Picault Damien, Raison Bertrand, Bacha Seddik, Labonne Antoine. Maximizing the power output of partially shaded photovoltaic plants through optimization of the interconnections among its modules. IEEE J Photovolt 2012;2(2):154–63.

[42] Nguyen Dzung, Lehman Brad. An adaptive solar photovoltaic array using model-based reconfiguration algorithm. IEEE Trans Industr Electron 2008;55(7):2644–54.

[43] Alahmad Mahmoud, Chaaban Mohamed Amer, Lau Su kit, Shi Jonathan, Neal Jill. An adaptive utility interactive photovoltaic system based on a flexible switch matrix to optimize performance in real-time. Sol Energy 2012;86:951–63.

[44] Velasco-Quesada Guillermo, Guinjoan-Gispert Francisco, Piqué-López Robert, Román-Lumbreras Manuel, Conesa-Roca Alfonso. Electrical PV array reconfiguration strategy for energy extraction improvement in grid-connected PV systems. IEEE Trans Industr Electron 2009;56(11):4319–31.

[45] Obane Hideaki, Okajima Keiichi, Oozeki Takashi, Ishii Takafumi. PV system with reconnection to improve output under nonuniform illumination. IEEE J Photovolt 2012;2(3):341–7.

[46] Salameh Ziyad M, Dagher Fouad. The effect of electrical array reconfiguration on the performance of a PV-powered volumetric water pump. IEEE Trans Energy Convers 1990;5(4):653–8.

[47] Storey Jonathan, Wilson Peter, Bagnall Darren. Improved optimization strategy for irradiance equalization in dynamic photovoltaic arrays. IEEE Trans Power Electron 2013;28(6):2946–56.

[48] Storey Jonathan, Wilson Peter R, Bagnall Darren. The optimized-string dynamic photovoltaic array. IEEE Trans Power Electron 2014;29(4):1768–76.

[49] La Manna Damiano, Vigni Vincenzo Li, Sanseverino Eleonora Riva, Di Dio Vincenzo, Romano Pietro. Reconfigurable electrical interconnection strategies for photovoltaic arrays: a review. Renew Sustain Energy Rev 2014;33:412–26.

[50] Romano Pietro, Candela Roberto, Cardinale Marzia, Vigni Vincenzo Li, Musso Domenico, Sanseverino Eleonora Riva. Optimization of photovoltaic energy production through an efficient switching matrix. J Sustain Dev Energy, Water Environ Syst 2013;1(3):227–36.

[51] Vaishnavi Ms, Deshpande P, Bodkhe SB. Review on effect of partial shading on photovoltaic array configurations. Int J Eng Res Appl (IJERA) 2014. ISSN 2248-9622.

[52] Carotenuto Pietro Luigi, Curcio Salvatore, Manganiello Patrizio, Petrone Giovanni, Spagnuolo Giovanni, Vitelli Massimo. Algorithms and devices for the dynamical reconfiguration of PV arrays. PCIM 2013, Nuremberg; May 14–16, 2013. p. 765–72.

[53] Balato M, Manganiello P, Vitelli M. Fast dynamical reconfiguration algorithm of PV arrays. EVER 2014, Monaco; March 25–27, 2014. p. 1–8.

[54] Website: http://www.bitronenergy.com.

[55] Sánchez-Friera P, Piliougine M, Peláez J, Carretero J, de Cordona M Sidrach. Analysis of degradation mechanisms of crystalline silicon PV modules after 12 years of operation in Southern Europe. Prog Photovoltaics Res Appl 2011;19(6):658–66.

[56] Kaplani E. Detection of degradation effects in field-aged c-Si solar cells through IR thermography and digital image processing. Int J Photoenergy 2012:1–11.

[57] Garcıa M, Marroyo L, Lorenzo E, Marcos J, Perez M. Observed degradation in photovoltaic plants affected by hot-spots. Progr Photovolt: Res Appl 2013. n/a–n/a.

[58] King DL, Quintana MA, Kratochvil JA, Ellibee DE, Hansen BR. Photovoltaic module performance and durability following long-term field exposure. Prog Photovoltaics Res Appl 2000;8(2):241–56.